Tropopause Structure and the Role of Eddies

JACOB HAQQ-MISRA AND SUKYOUNG LEE

The Pennsylvania State University, University Park, Pennsylvania

DARGAN M. W. FRIERSON

University of Washington, Seattle, Washington

(Manuscript received 21 March 2011, in final form 1 July 2011)

ABSTRACT

This paper presents a series of dynamical states using an idealized three-dimensional general circulation model with gray radiation and latent heat release. Beginning with the case of radiative–convective equilibrium, an eddy-free two-dimensional state with zonally symmetric flow is developed, followed by a three-dimensional state that includes baroclinic eddy fluxes. In both dry and moist cases, it is found that the deepening of the tropical tropospheric layer and the shape of the extratropical tropopause can be understood through eddy-driven processes such as the stratospheric Brewer–Dobson circulation. These results suggest that eddies alone can generate a realistic tropopause profile in the absence of moist convection and that stratospheric circulation is an important contributor to tropopause structure.

1. Introduction

The boundary between the troposphere and stratosphere is known as the tropopause and has been empirically characterized in a number of ways that include an abrupt change of atmospheric lapse rate, an increase in static stability, a rapid change in potential vorticity, and a difference in chemical composition. Prominent atmospheric circulations, such as the Hadley circulation, as well as most weather systems are confined to the troposphere, and air parcels in the troposphere that rise to the tropopause lose most of their water so that the stratosphere is comparatively dry. Nevertheless, the troposphere and stratosphere are known to interact significantly with one another, such as through the exchange of mass, momentum, and energy (Holton et al. 1995; Stohl et al. 2003).

The time-mean structure of the tropopause can be approximated to first order as the result of radiative forcing only (Manabe and Wetherald 1967), but an atmosphere in pure radiative equilibrium is convectively unstable near the surface. The use of a convective adjustment mechanism restores stability and allows tropopause height to be determined as the result of both radiation and convection (Manabe and Strickler 1964; Held 1982; Thuburn and Craig 1997, 2000). This model is often applied in the tropics (latitude $\phi < 30°$), where moist convection raises tropopause heights to produce a sharp discontinuity between the tropopause in the moist tropics and the drier extratropics (Held 1982; Xu and Emanuel 1989; Highwood and Hoskins 2006). This "subtropical jump" in tropopause height (at $\phi \approx 30°$) is also evident in observations (Hoerling et al. 1991; Hoinka 1998; Seidel and Randel 2007).

Radiative–convective equilibrium cannot fully explain the shape of the extratropical tropopause because the extratropics ($\phi > 30°$) are baroclinically unstable. It has been widely discussed that baroclinic eddies modify lapse rate through horizontal and vertical heat transport to sharpen and raise the extratropical tropopause (Held 1982; Lindzen 1993; Schneider 2004). This effect of baroclinic eddies on extratropical tropopause height is also evident in numerical models (Gutowski 1985; Gutowski et al. 1992; Egger 1995; Ambaum 1997; Barry et al. 2000; Haynes et al. 2001; Wirth 2003; Schneider 2004; Wirth and Szabo 2007; Schneider and O'Gorman 2008) and observational analyses (Birner et al. 2002; Dell'Aquila et al. 2007). Stratospheric processes are also thought to contribute to tropopause structure in the extratropics (Gabriel et al. 1999; Kirk-Davidoff and Lindzen 2000; Thuburn and Craig 2000; Bordi et al. 2002; Seidel and

Corresponding author address: Jacob Haqq-Misra, The Pennsylvania State University, 201 Willard Building, University Park, PA 16802.
E-mail: haqqmisra@psu.edu

DOI: 10.1175/JAS-D-11-087.1

Randel 2006; Son et al. 2007; Birner 2010) through the Brewer–Dobson circulation (Holton et al. 1995). All of these features of the tropical and extratropical tropopause are evident in our model results. However, we also find that the same features, including a raised tropical tropopause and subtropical jump, occur under dry conditions in the absence of moist convection. This suggests that previous hypotheses for tropopause height may overestimate the role of moisture and underestimate the role of eddies in maintaining tropical tropopause structure.

In this paper we investigate the explicit effect of baroclinic eddies on the height of the tropical and extratropical tropopause. To make consistent comparisons between eddy-free and eddy-permitting atmospheres, we develop a hierarchy of three dynamical states: radiative–convective equilibrium (RCE), a two-dimensional state (2D), and a three-dimensional state (3D). We initialize RCE by suppressing explicit motion, including eddies and the mean meridional circulation. Adding in advection by overturning meridional circulation to RCE yields the 2D state, which is baroclinically unstable and still lacks transport by eddies. The final 3D state is then obtained when the 2D state is perturbed so that eddies develop. By comparing these RCE, 2D, and 3D cases under both dry and moist conditions, we find that midlatitude eddy fluxes significantly contribute to the structure of both the tropical and extratropical tropopause.

2. Dynamical hierarchy

The general circulation model (GCM) used in these calculations is based on the spectral model developed at the Geophysical Fluid Dynamics Laboratory (GFDL) (Gordon and Stern 1982; Anderson et al. 2004) and is thoroughly described by Frierson et al. (2006) and Haqq-Misra (2010). This GCM builds upon the hydrostatic primitive equation dynamical core of Held and Suarez (1994) by including latent heat release by large-scale condensation. In addition, gray radiation directly forces the atmosphere, instead of Newtonian relaxation to a fixed profile, and an explicit boundary layer scheme replaces Rayleigh damping as surface friction. The atmosphere is assumed to be transparent to solar radiation so that the surface slab ocean absorbs sunlight in a perpetual equinox configuration. Optical depth values at the equator and pole are specified at the surface, and the vertical profile of optical depth is specified as a function of pressure. These radiation parameters are identical to those described in detail by Frierson et al. (2006).

This model is still highly idealized because water vapor content has no effect on the radiation budget, and the surface is parameterized as a mixed-layer slab ocean of constant heat capacity and albedo. For these calculations we use $N_L = 25$ vertical levels with sigma coordinates spaced according the expression $\sigma = \exp[-5(0.05\tilde{z} + 0.95\tilde{z}^3)]$, where $\tilde{z}$ is equally spaced in the interval $0 \leq \tilde{z} < 1$, and a spectral dynamical core with triangular truncation at wavenumber 42 (i.e., T42, which approximately corresponds to 2.8° horizontal resolution). Each simulation is run for a 3000-day spinup period to reach a statistically steady state. We then use the subsequent 1000 days of model runtime in our analysis.

The RCE state is reached by setting $\mathbf{v} \cdot \nabla T = \mathbf{v} \cdot \nabla \mathbf{v} = \nabla p = 0$ in the primitive equations so that the horizontal advection of temperature and momentum, along with the pressure gradient, is zero. (It would seem that RCE could be achieved simply by setting all horizontal and vertical winds to zero, but such a configuration is numerically unstable in a GCM because pressure gradients are still present.) The model is initialized with a constant temperature of 264 K at all grid points, and no perturbation is introduced into the system at initialization. The resulting steady state has no zonal or meridional wind and is conceptually equivalent to applying a one-dimensional radiative convective model to calculate a vertical temperature profile at every surface grid point. To reach the 2D state, no terms in the primitive equations are suppressed, but we still refrain from perturbing any zonally asymmetric motion in the model at initialization. This yields a baroclinically unstable climate state with zonally symmetric steady flow and no eddy fluxes. The final 3D climate state resembles an idealized earth climate and is reached by numerically perturbing the vorticity field at initialization to induce the formation of baroclinic eddies.

Because radiative transfer strongly destabilizes the atmosphere to convection, some convective parameterization must be used in all simulations. In the dry cases, we apply convective adjustment toward a dry adiabat (Manabe et al. 1965) by mixing unstable layers while conserving the vertical integral of potential temperature with respect to pressure. For our moist cases, we use a simplified penetrative adjustment scheme (Betts 1986) that is fully developed by Frierson (2007). This penetrative adjustment scheme uses a reference relative humidity of 80% to calculate an adjustment to temperature that satisfies conservation of enthalpy [we use the ''shallower'' scheme developed by Frierson (2007)]. We initially attempted to use a moist convective adjustment scheme as a counterpart to dry convective adjustment; however, moist convective adjustment proved unsuitable for producing a stable moist RCE state because the lack of meridional transport in RCE causes water vapor to accumulate in the tropical troposphere. [This is because water vapor content is variable in our model configuration and therefore requires either poleward transport or an explicit cloud scheme to stabilize RCE (Emanuel

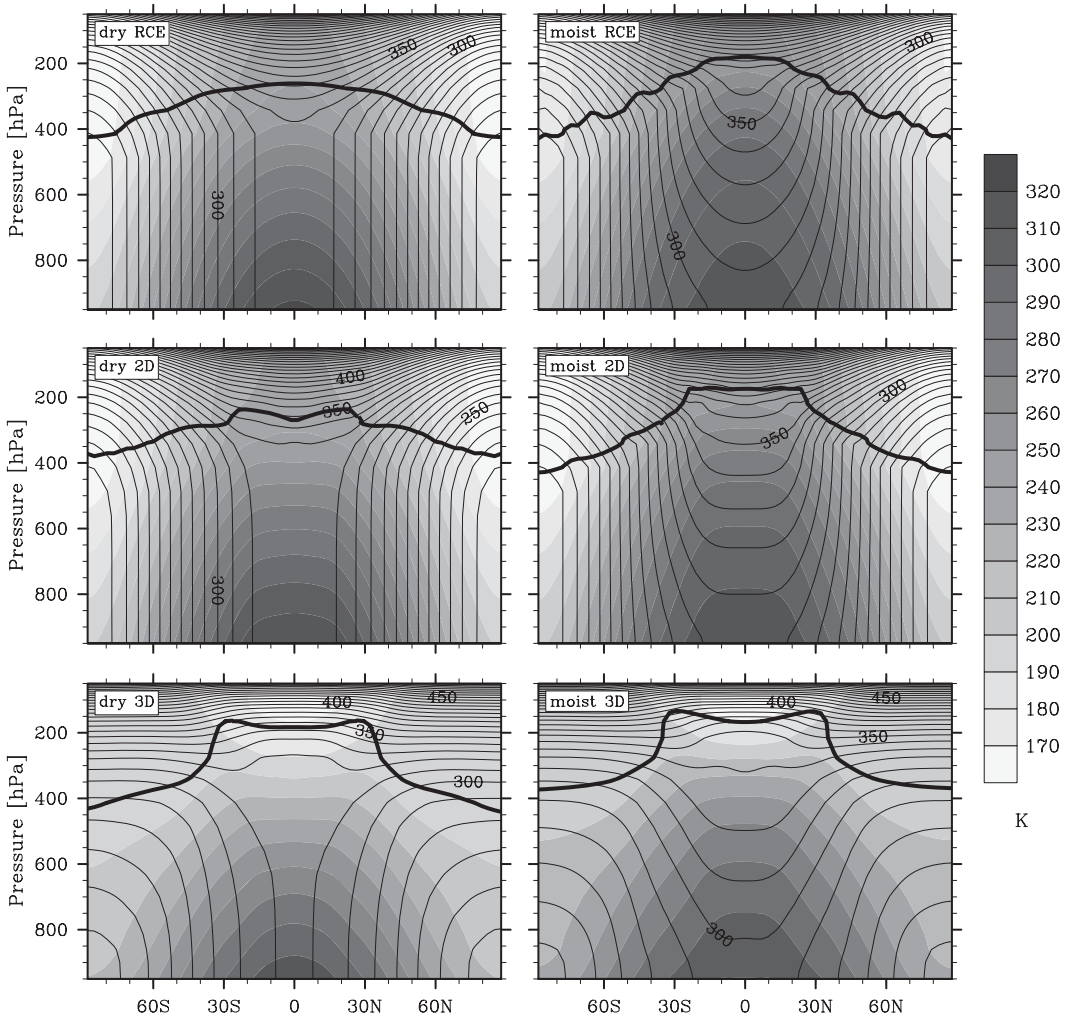

FIG. 1. $\overline{T}$ (shading) and $\overline{\theta}$ (lines) for dry and moist RCE, 2D, and 3D cases with a contour interval of 10 K. The dark curve indicates the height of the tropopause according to the WMO lapse rate definition.

1994).] By contrast, a simplified penetrative adjustment scheme adequately stabilizes the model atmosphere for all our dynamical configurations, which makes it a suitable choice for our moist simulations.

A summary of the RCE/2D/3D hierarchy is given in Fig. 1, which shows the zonal mean potential temperature θ for all three dynamical states, with dry cases in the left column and moist cases in the right column. Each panel also includes a tropopause (dark curve) defined by the World Meteorological Organization (WMO 1957) with a typical lapse rate of 2 K km^{-1}. Dry RCE is characterized by a dry adiabatic lapse rate $d\theta/dp = 0$ (where p is pressure) in the troposphere, while the addition of advection in dry 2D allows an overturning meridional circulation to develop. The corresponding moist cases fall nearly along moist adiabats in the troposphere (not shown), and tropopause heights are generally higher than the dry counterparts. When eddies are included in 3D, a more realistic meridional variation in tropopause height appears. We have also plotted an overlay of the RCE, 2D, and 3D tropopauses under dry and moist conditions in Fig. 2 to highlight the changes in tropopause height among these three dynamical configurations. Our model results differ in this respect from other idealized GCM calculations (e.g., Held and Suarez 1994) because of our use of explicit radiative transfer and boundary layer processes. Other GCM studies (e.g., Schneider and O'Gorman 2008) present a subset of some of the calculations shown here, although they do not systematically compare dry and moist cases in order to isolate the effects of moisture. Indeed, our construction of this single-model dynamical hierarchy allows us to systematically explore the explicit effects of baroclinic eddies on atmospheric structure.

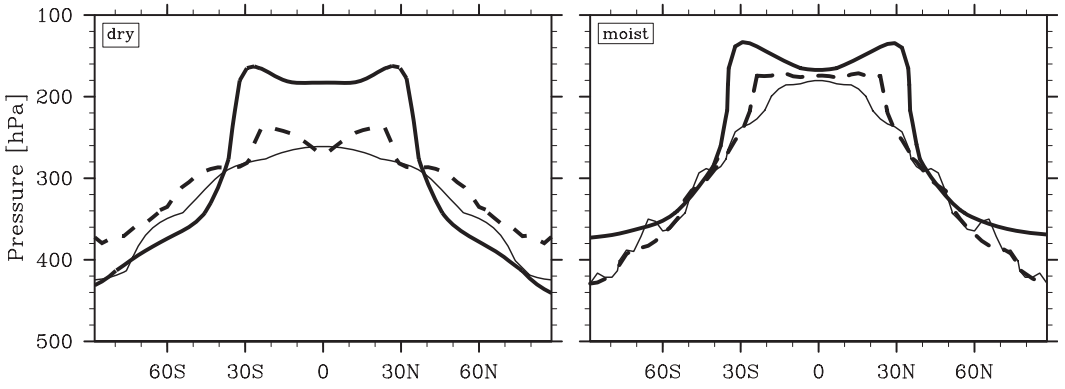

FIG. 2. Tropopause heights according to the WMO lapse rate definition for the RCE (thin line), 2D (dashed line), and 3D (thick line) dynamical states under (left) dry and (right) moist conditions.

3. Tropical tropopause

Conventional wisdom attributes the height of the tropical tropopause to the presence of moist convection, which is illustrated in our moist suite of models. (Our analysis in this paper is based on a tropopause defined by lapse rate and neglects the presence of the tropical tropopause layer.) Moist RCE shows a tropopause height that peaks at the equator, where the greatest amount of moisture is present. This moist RCE tropopause then declines in height throughout the wet tropics and into the drier extratropics. (The bumps in the moist RCE tropopause profile result from the fact that we are forcing the GCM into an RCE state that would otherwise be numerically unstable.) In moist 2D, an overturning meridional circulation develops that mixes water vapor within the tropics (not shown). Eddies are still absent in moist 2D, but the tropopause is now a constant height throughout the tropics. When eddies are included in moist 3D, the subtropical tropopause near $\phi \approx 30°$ rises slightly, which produces the characteristic time-mean tropopause shape from observations.

Contrary to this conventional argument, a realistic meridional variation in tropopause height also can be achieved in a dry atmosphere with the complete absence of moist convection. [Thuburn and Craig (1997) hint at this behavior, where some of their drier model experiments show a slightly lower tropopause that retains many realistic structural features.] Our state of dry RCE shows maximum heating at the equator and a tropopause that smoothly declines toward the poles. The overturning circulation in dry 2D reduces the tropical horizontal temperature gradient so that the tropopause flattens somewhat throughout the tropics. Our dry 2D state is somewhat approximate to our dry RCE state, though, and does not show a significant rise in tropical tropopause heights as in moist 2D. However, when we add eddies to our dry model in the dry 3D state, we find a tropopause with a shape quite similar to that of moist 3D. The height of the dry 3D tropopause in the tropics is nearly as high as the moist 3D tropopause, and the abrupt subtropical jump is also evident. [It is also worth noting that the meridional temperature gradient is reduced in moist 3D when compared to its dry counterpart because the inclusion of latent heat transport enhances the net poleward heat transport by baroclinic eddies. Although this behavior is worthy of future investigation (e.g., Frierson et al. 2007), such calculations are beyond the scope of the present study.] The realistic shape of our dry 3D tropopause occurs in the complete absence of moisture, which suggests that tropospheric and stratospheric eddies alone can constrain the shape of the tropical tropopause.

The effect of eddies on tropopause shape can be understood by considering the structure of potential temperature in the atmosphere. To conduct our analysis, we interpret the difference δ of a field χ between 2D and 3D dynamical states as the net eddy effect:

$$\delta(\chi) = \chi_{3D} - \chi_{2D}. \tag{1}$$

This allows us to explicitly calculate the contribution of eddies to any atmospheric quantity. We first show the net eddy effect of potential temperature $\delta(\overline{\theta})$ in Fig. 3 under dry and moist conditions. In both instances we see that eddies yield cooling in the tropics, with the steepest vertical gradient of cooling just beneath the tropical tropopause. We have defined the tropopause in terms of lapse rate $\partial\overline{\theta}/\partial p$, so we can examine the contribution of eddies to the vertical temperature gradient by considering the static stability of the atmosphere. As a measure of static stability, we use the quantity $\overline{N}^2$, defined as

$$\overline{N}^2 = g\frac{\partial \ln\overline{\theta}}{\partial z} = \frac{g^2 p}{R_d T}\frac{\partial \ln\overline{\theta}}{\partial p}, \tag{2}$$

which describes statically stable conditions for $\overline{N}^2 > 0$ and statically unstable conditions for $\overline{N}^2 < 0$. (Here g is

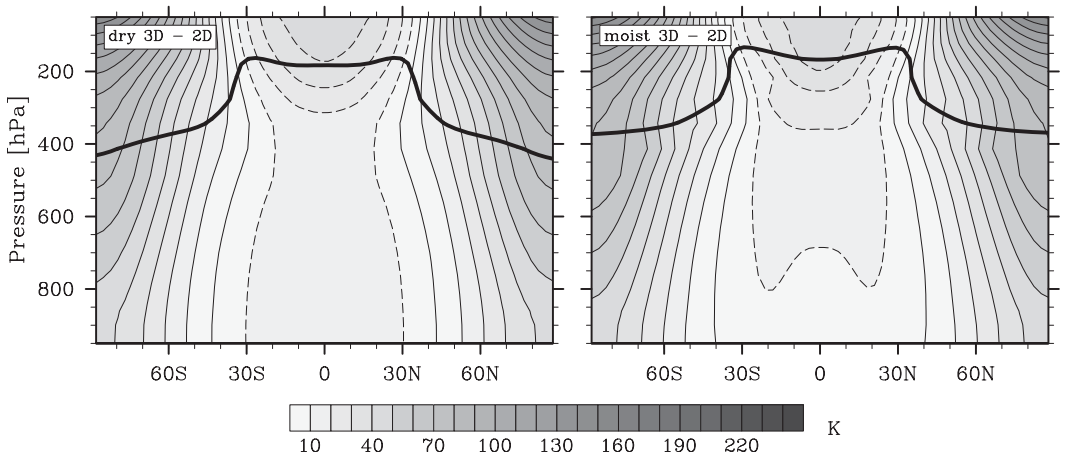

FIG. 3. $\delta(\overline{\theta})$ for dry and moist cases. Dashed curves indicate negative values, and shading shows $|\delta(\overline{\theta})|$. Contours are drawn every 10 K, and the dark line follows the tropopause.

a constant gravitational acceleration, z is height, T is temperature, R_d is the specific gas constant for dry air, and overbars denote a zonal mean.) The change in static stability due to the presence of eddies can be described by the net eddy effect $\delta(\overline{N}^2)$. We plot $\overline{N}^2$ as well as $\delta(\overline{N}^2)$ for our 2D and 3D cases in Fig. 4. In the tropics, the stratospheric cooling by eddies corresponds to a decrease static stability $[\delta(\overline{N}^2) < 0]$ in the upper troposphere through a reduction in the vertical temperature gradient $\partial\theta/\partial z$, whereas it corresponds to an increase static stability $[\delta(\overline{N}^2) > 0]$ in the lower stratosphere due to the decrease in temperature. Together, these changes lift the tropical tropopause from the eddy-free 2D state to the eddy-permitting 3D state. This result is consistent with the work of Birner (2010), who also points out that the region of negative net eddy effect beneath the tropopause helps sharpen the subtropical jump. Likewise, the observational analysis by Pan et al. (2004) also finds that an abrupt change in the magnitude of $\overline{N}^2$ is associated with sharpness in tropopause structure. Under both dry and moist conditions, we find that eddies lift the height of the tropical tropopause through an increase in static stability above the tropopause and a decrease in static stability beneath.

One way that eddies modify static stability in the stratosphere is through the Brewer–Dobson circulation, which we describe using the residual meridional mass streamfunction (see below). On the earth, this circulation provides equator-to-pole mass transport with a maximum in the winter hemisphere (Brewer 1949; Holton et al. 1995; Callaghan and Salby 2002; Austin and Li 2006) and is driven in part by the convergence of the eddy heat flux $\overline{v'\theta'}$ and the eddy momentum flux $\overline{u'v'}$ (by modifying horizontal motion $\overline{v}$ and vertical motion $\overline{\omega}$). The equator-to-pole motion of the Brewer–Dobson circulation suggests that a corresponding cooling in the equatorial stratosphere and warming in the polar stratosphere may provide one mechanism by which stratospheric eddies can contribute to tropopause structure. To explore this hypothesis, we calculate the residual meridional circulation in the stratosphere as a proxy to the Brewer–Dobson circulation.

In general, the residual circulation approximates mass transport across isentropes, which is relevant for exchange between the stratosphere and troposphere. We can describe the residual meridional circulation with a transformed Eulerian mean formulation (Eliassen and Palm 1961; Andrews and McIntyre 1976) that approximates mean meridional flow associated with diabatic processes. Following Edmon et al. (1980), we define the components of the residual velocity as

$$\overline{v}^* = \overline{v} - \frac{\partial}{\partial p}\left(\frac{\overline{v'\theta'}}{\partial\overline{\theta}/\partial p}\right), \tag{3}$$

$$\overline{\omega}^* = \overline{\omega} + \frac{1}{a\cos\phi}\frac{\partial}{\partial\phi}\left(\frac{\overline{v'\theta'}\cos\phi}{\partial\overline{\theta}/\partial p}\right), \tag{4}$$

which we can use to calculate the residual meridional circulation Ψ^* as

$$\Psi^* = \frac{2\pi a^2\cos\phi}{g}\int_0^{p'}\overline{v}^*\,dp, \tag{5}$$

where P' is a particular pressure level for the mean meridional circulation and a is planetary radius. The residual meridional streamfunction Ψ^* is shown in Fig. 5 for our 3D state with both contours and shading to enhance readability. [Because much of the residual circulation is driven by eddies, the change in residual circulation $\delta(\Psi^*)$ from 2D to 3D is similar to the total

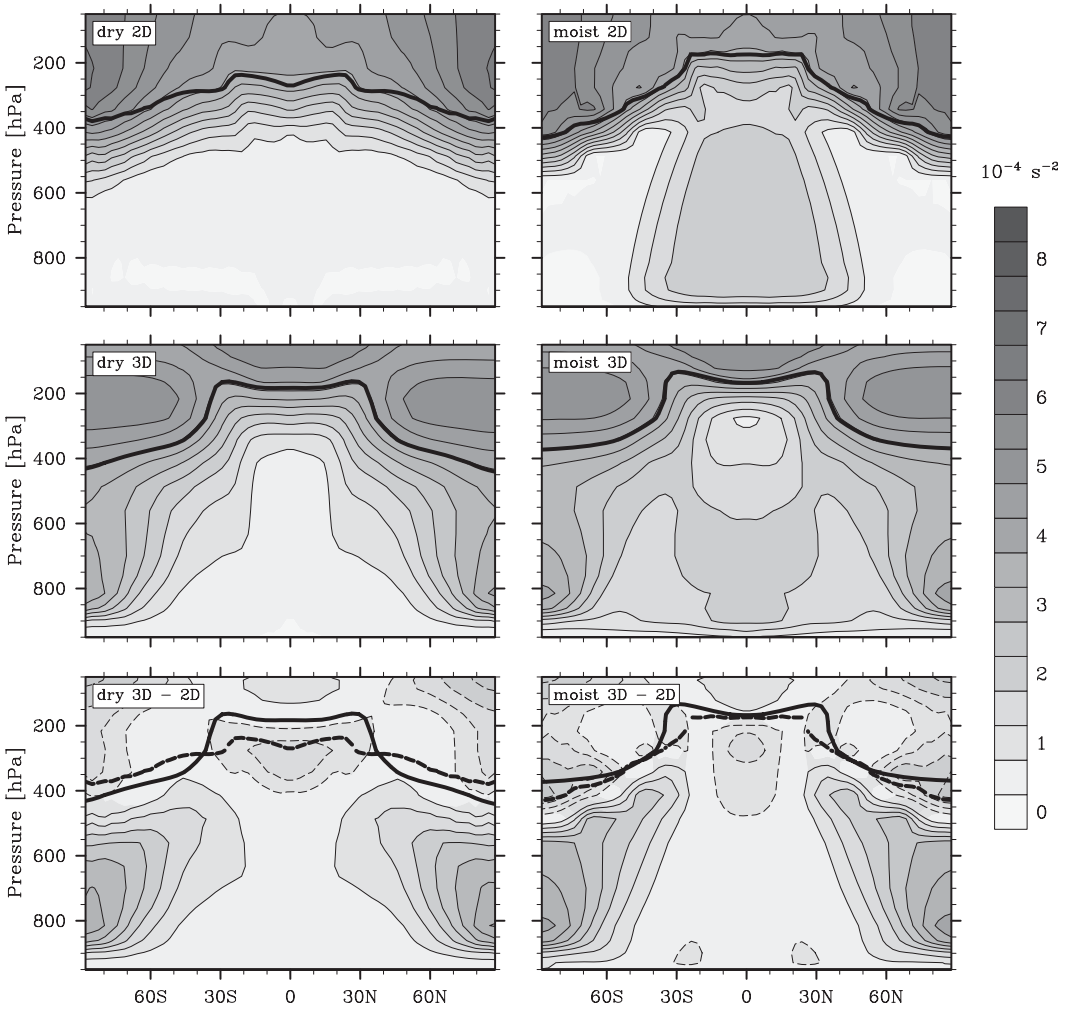

FIG. 4. $\overline{N}^2$ for dry and moist (top) 2D and (middle) 3D cases and (bottom) $\delta(\overline{N}^2)$ between the 3D and 2D cases. Contours are drawn at an interval of 5×10^{-5} s^{-2}. Dashed contours show negative values, and shading shows $|\overline{N}^2|$ and $|\delta(\overline{N}^2)|$. The dark solid line follows the 3D tropopause and the dark dashed line follows the 2D tropopause.

3D circulation of Fig. 5. The Ψ^* field for the eddy-free 2D state reduces to the mean meridional circulation (MMC) and is confined to a narrow band in the tropical troposphere. We have not included a plot of the MMC in this paper because it is tangential to the discussion of tropopause height, although we intend to investigate the role of eddies in the Hadley circulation in a future study.] The equator-to-pole transport mechanism discussed above for the stratosphere is evident in both the top and bottom rows of Fig. 5 along with vertical upwelling at equatorial latitudes. Note that even though the tropospheric residual circulation is stronger in dry 3D, the magnitude of the Brewer–Dobson circulation in the stratosphere is nearly identical between dry and moist 3D because the vertical stability $\partial\overline{\theta}/\partial p$ is similar in the relatively dry stratosphere of these two cases. We can compare $\delta(\overline{\theta})$ in Fig. 3 with Fig. 5 to see that the region of cooling just beneath and above the tropical tropopause corresponds to a rising branch of the residual circulation. The associated decrease in static stability $\delta(\overline{N}^2)$ beneath the tropical tropopause, seen in the bottom row of Fig. 4, results from a decrease in the vertical potential temperature gradient by this overturning circulation (also evident in Fig. 3)—although part of this response may also be due to eddy-driven changes in tropospheric longwave radiation. In this way we see that eddies can raise tropical tropopause heights out of the reach of convection (Birner 2010) through the Brewer–Dobson circulation, even in the absence of moisture.

4. Extratropical tropopause

The shape of the tropopause in the extratropics has been considered a result of baroclinic eddies (in part) at least since Held (1982). The influence of baroclinic eddies

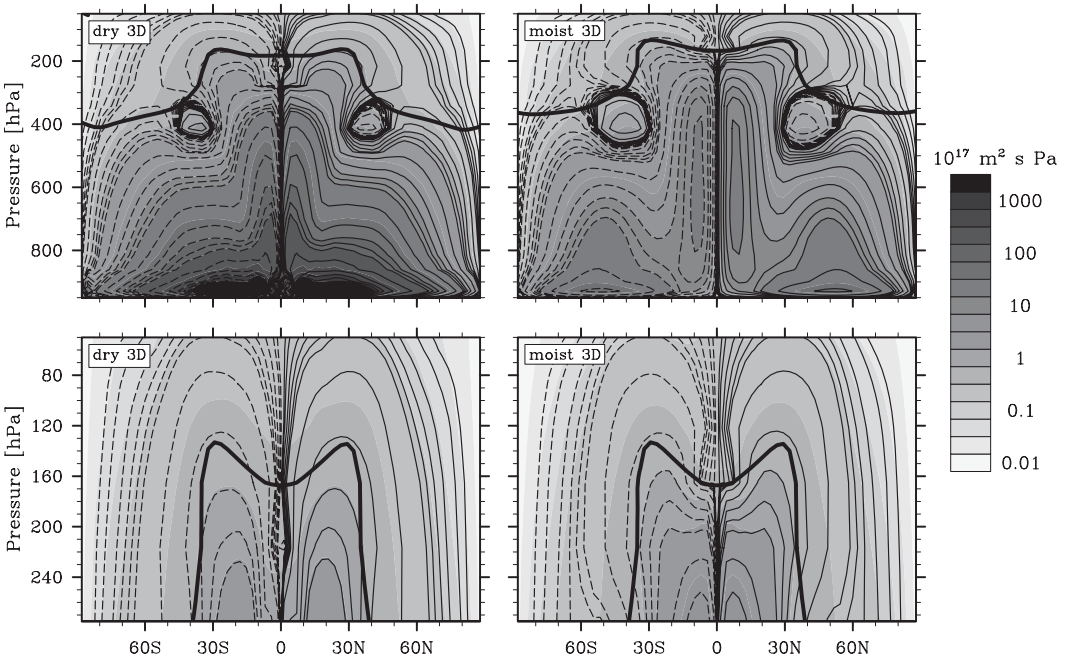

FIG. 5. Plots of Ψ^* (10^{17} m^2 s Pa). Contours are drawn irregularly according to $\pm\{1, 2, 4, 6, 8\} \times 10^n$, where $-2 \le n \le 4$, and dashed contours mark negative values. Shading follows the logarithmic scale on the side and indicates $|\Psi^*|$. (top) Plot for the full atmosphere, with a dark curve showing the tropopause, and (bottom) in the stratosphere only.

on extratropical tropopause structure can be seen from our dynamical hierarchy in Fig. 1. Our RCE and 2D states show nearly identical tropopause shape in the extratropics, where radiation and convection are the only constraining processes (in addition to some tropical heat transport from the mean meridional circulation in 2D). When we induce eddies under dry conditions to form our dry 3D state, we find that the tropopause lowers significantly throughout the entire extratropics. This contrasts with our moist 3D state, which shows a rise in polar tropopause height due to eddies. Baroclinic eddies evidently exert a different effect on extratropical tropopause structure based on the presence or absence of moisture. As we discuss below, the behavior of both our dry and moist 3D states can be attributed in part to a competition between the Brewer–Dobson circulation and the tropospheric eddy heat flux.

The prominence of baroclinic eddies in shaping the extratropical tropopause is illustrated by static stability $\overline{N}^2$ shown in Fig. 4, which shows that eddies act to stabilize the stratification in the extratropics. The regions of negative static stability net eddy effect $\delta(\overline{N}^2)$ above the extratropical tropopause are almost identical in strength and shape between our moist and dry cases. This is associated with warming and an increase in lapse rate in the extratropical stratosphere that lowers the extratropical tropopause, which can be explained as warming by increased upward infrared radiation and the downward motion of the Brewer–Dobson circulation. Eddy-driven processes lead to a rise in tropospheric temperatures, which causes an increase in upward infrared radiation into the stratosphere. The resulting stratospheric warming is similar between our dry and moist calculations because moist static energy fluxes are nearly equal in the two cases (Frierson et al. 2007), which ensures that upward infrared radiation into the stratosphere is also equal. The Brewer–Dobson circulation also contributes to the structure of temperature in the stratosphere and likewise shows equivalent tendencies between our dry and moist cases (Fig. 5). This stratospheric warming is certainly important in shaping the extratropical tropopause, but some other mechanism must also be present to explain the difference in tropopause slope between our dry and moist simulations.

We describe our hypothesis for the shape of the extratropical tropopause as a schematic diagram shown in Fig. 6. The top panel considers dry conditions where tropospheric heating processes are limited to radiation, dry convective adjustment, and the boundary layer. In this case, the stratospheric residual circulation (along with changes in upward infrared radiation) may cause cooling at low latitudes and warming at high latitudes that exceed the corresponding warming and cooling from poleward sensible heat fluxes in the troposphere. This would cause a lowering of the extratropical tropopause. This lowering of the extratropical tropopause from dry 2D to dry 3D is consistent with our dry calculations shown

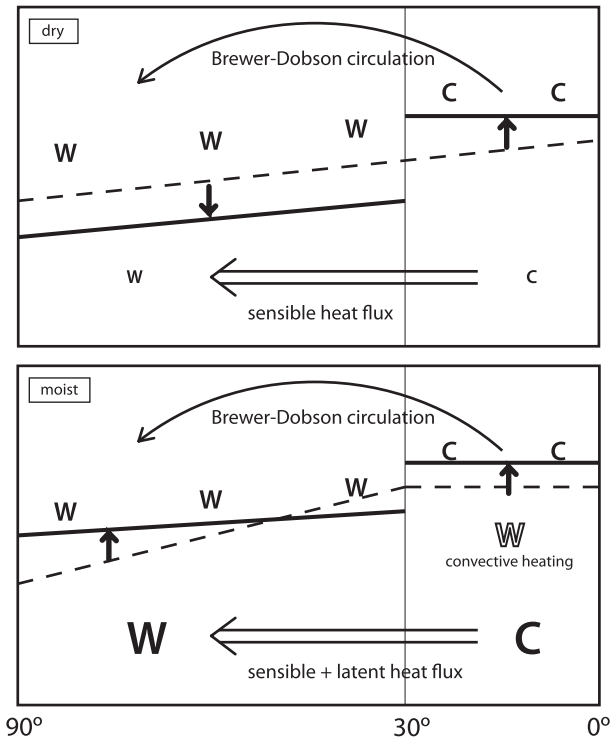

FIG. 6. A schematic diagram illustrating the influence of the residual circulation on tropopause height. The dashed line shows the 2D tropopause and the dark solid line shows the 3D tropopause. (top) Results for dry conditions, where stratospheric cooling in the tropics results in a rise in the tropical tropopause, while the corresponding warming at higher latitudes from the Brewer–Dobson circulation causes the extratropical tropopause to sink. (bottom) Results for moist conditions, where the addition of convective heating causes an even greater rise in tropical tropopause height. Likewise, the presence of latent heat fluxes results in a rise in the extratropical tropopause.

in Fig. 1. Under moist conditions, however, the presence of moist convection and latent heat fluxes may cause eddies to raise the extratropical tropopause rather than lower it. We illustrate this response of the moist tropopause in the lower panel of Fig. 6. The strength of the stratospheric warming is similar between our dry and moist cases, as discussed above, so the resulting warming and cooling in the stratosphere could likewise be similar. In the tropics, moist processes result in convective heating that cause the tropical tropopause to rise above its dry 3D counterpart. Moist processes also create an additional poleward and upward flux of sensible heat, as evidenced by greater eddy-driven dynamic warming for the moist case than for the dry case. In this case, low-latitude cooling and high-latitude warming in the troposphere should dominate that in the stratosphere and cause the extratropical tropopause to rise. This raising effect of baroclinic eddies is also consistent with our moist calculations in Fig. 1. According to our hypothesis, the shape of the extratropical tropopause is constrained by a competition between warming in the stratosphere and the influence of latent heat fluxes in the troposphere.

We can examine the magnitude of this heating by calculating the net eddy effect of dynamical heating and physical heating. We define dynamical heating $\overline{\mathfrak{D}}$ as the sum of advection and pressure work terms,

$$\overline{\mathfrak{D}} = -\overline{\mathbf{v}\cdot\nabla T} + \frac{\overline{R_d T\omega}}{c_p P}, \tag{6}$$

so that the net eddy effect of dynamical heating is $\delta(\overline{\mathfrak{D}})$. We represent eddy heating from nonradiative physical processes as $\delta(\overline{Q}_{\text{norad}})$. Here we have written heating due to nonradiative physical processes as $\overline{Q}_{\text{norad}} = \overline{Q}_{\text{conv}} + \overline{Q}_{\text{vdif}} + \overline{Q}_{\text{lsc}}$ (so that total heating due to physical processes $\overline{Q} = \overline{Q}_{\text{norad}} + \overline{Q}_{\text{rad}}$), where the three terms on the right-hand side represent the temperature tendency due to convection, vertical diffusion, and large-scale condensation, respectively. Temperature change caused by latent heat transport is included in $\overline{Q}_{\text{conv}}$ and $\overline{Q}_{\text{lsc}}$. We plot $\delta(\overline{\mathfrak{D}})$ and $\delta(\overline{Q}_{\text{norad}})$ as well as the total nonradiative net eddy effect $\delta(\overline{\mathfrak{D}}) + \delta(\overline{Q}_{\text{norad}})$ in Fig. 7 for dry and moist conditions. If we examine the top row showing $\delta(\overline{Q}_{\text{norad}})$, we see that warming and cooling from physical processes are largely confined to heights below 400 hPa, which suggests that such processes have little direct impact on the stratospheric energy budget. Warming by moist convective adjustment does allow tropical heights to rise higher than under dry convective adjustment. Moisture also causes $\overline{Q}_{\text{norad}}$ to extend farther poleward and upward. Consistent with this influence of moisture, the middle row of Fig. 7 shows that dynamical warming $\delta(\overline{\mathfrak{D}})$ is greater in the extratropical troposphere when moisture is included. The combined effect of these physical and dynamical processes $\delta(\overline{\mathfrak{D}}) + \delta(\overline{Q}_{\text{norad}})$ in the bottom row of Fig. 7 also shows a greater net warming beneath the extratropical tropopause when moisture is present. Warming and cooling in the stratosphere is similar between moist and dry conditions, which suggests that tropospheric processes contribute to the difference in the eddy-driven determination of tropopause slope.

We describe the shape of the tropical and extratropical tropopause as a result of eddy-driven processes that include the Brewer–Dobson circulation. The change in upwelling motion of the residual circulation in the tropical stratosphere (as evident in Fig. 5) reduces the vertical temperature gradient and causes tropopause heights to rise, while downwelling motion toward the poles yields both an increase in temperature and an increase in vertical temperature gradient. Eddies likewise increase the vertical temperature gradient in the extratropical troposphere and give the tropopause its characteristic shape. This leads

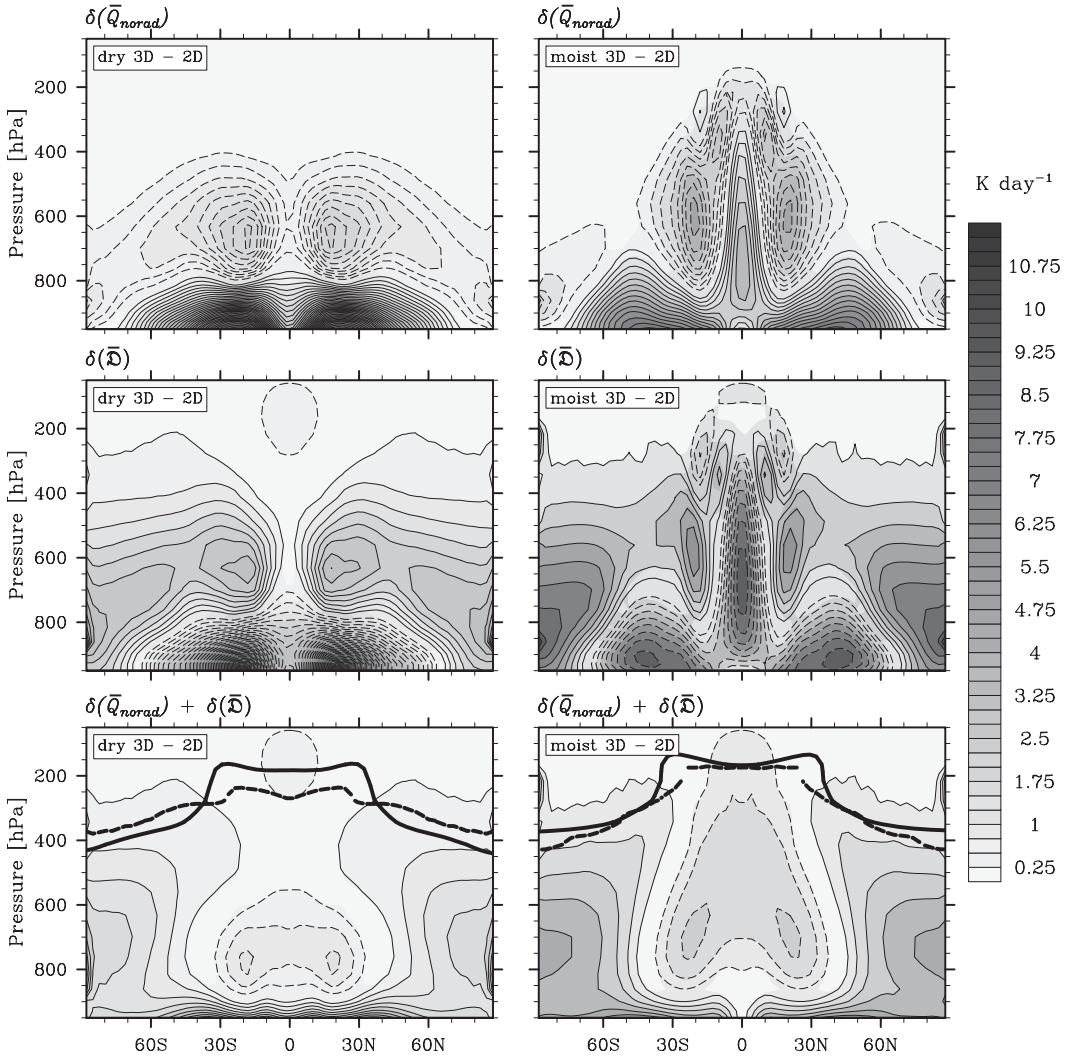

FIG. 7. (top) $\delta(\overline{Q}_{\text{norad}})$, (middle) $\delta(\overline{\mathfrak{D}})$, and (bottom) $\delta(\overline{\mathfrak{D}}) + \delta(\overline{Q}_{\text{norad}})$, for (left) dry and (right) moist cases. Dashed curves indicate negative values, and shading marks $|\delta(\overline{\mathfrak{D}}) + \delta(\overline{Q}_{\text{norad}})|$. The dark solid line follows the 3D tropopause and the dark dashed line follows the 2D tropopause. Contours are drawn every 0.25 K day^{-1}.

to a steepening of the tropopause in dry 3D and flattening in moist 3D. Our moist simulations contain a latent poleward heat flux in addition to the sensible heat flux in our dry cases, which causes the amount of warming due to eddies in the extratropical troposphere to be greater in moist 3D than in dry 3D so that the moist tropopause flattens while the dry tropopause steepens. We thus see that eddies act to sharpen the tropical and subtropical features of the tropopause and steepen the extratropical tropopause in a competition with latent heat fluxes.

5. Transient evolution

So far our analyses have been confined to the time-mean state of our dynamical hierarchy, but the temporal evolution of tropopause height in response to eddies provides us with further insight. We begin with a statistically steady-state 2D simulation, as in the middle row of Fig. 1, and perturb this dynamical state to induce the formation of baroclinic eddies. We make this numerical perturbation using a Mersenne twister pseudorandom number generator to adjust either vorticity $\zeta_k \rightarrow \zeta_k + \tilde{\zeta}$ by a stochastic value $10^{-8} < \tilde{\zeta} < 10^{-6}$ s^{-1} in the lowest three layers $N_L - 2 \leq k \leq N_L$ or temperature $T_k \rightarrow T_k + \tilde{T}$ by a stochastic value $0 < \tilde{T} < 1$ K in all vertical levels $0 \leq k \leq N_L$ at $\phi = 90°$S and longitude $\lambda = 0°$. This perturbs our baroclinically unstable 2D dynamical state to form baroclinic eddies and evolve toward a 3D dynamical configuration. Because individual simulations of adjustment from 2D to 3D dynamical states are

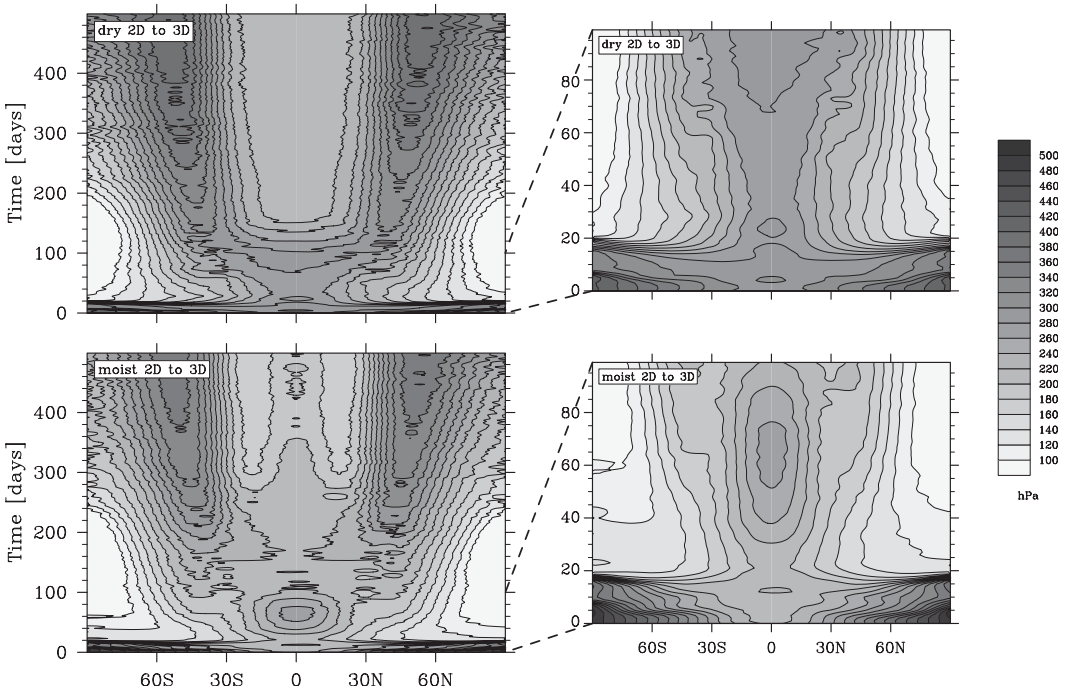

FIG. 8. Time evolution of zonal mean tropopause height for 500 days from the 2D to 3D dynamical state for an ensemble of calculations under (top) dry and (bottom) moist conditions. (right) Magnification of the first 100 days of evolution. Shaded contours are drawn at an interval of 50 hPa.

sensitive to initial conditions, we calculate a 10-member series of these random perturbations in order to find an ensemble mean tropopause height. (The magnitude of our perturbations is relatively small with $\tilde{\zeta} < \zeta_k$, so we are reasonably confident that our calculations should all converge to a similar steady state. If we were to increase our perturbations to make the magnitude of perturbation about equal to vorticity in our model layer so that $\tilde{\zeta} \approx \zeta_k$, then we could end up with several different final steady states or a final climate configuration that does not resemble our 3D state.)

We show transient evolution of zonal mean tropopause height from 2D to 3D under dry and moist conditions with our 10-member ensemble in Fig. 8, where shading indicates the pressure level of the tropopause at a given latitude and time. The tropical tropopause in both cases rises in response to eddies relatively quickly and is close to a steady state after the 500th day of evolution. (It should also be noted that the equatorial tropopause lowers between days 30 and 100, particularly in the moist case. This is largely in response to a decrease in tropical temperature from the eddy-driven poleward heat transport. The equatorial tropopause then slowly rises on a longer time scale as the Brewer–Dobson circulation develops and cools the lower stratosphere.) The extratropics, on the other hand, take much longer to equilibrate and are not yet at a steady state at the end of our 500-day window. We see that the subtropical jump begins to take shape by 150 days, although the regions poleward of $\phi \approx 45°$ latitude are markedly higher than their time-mean 3D configuration. In general, tropopause heights in the tropics tend to reach their near-final level much more quickly than in the extratropics, although the entire atmosphere requires about 1000 days to reach a statistically steady state. We can also see that the first 30 days of model evolution include a much more rapid adjustment period to the onset of baroclinic eddies that precedes the gradual refining of tropopause shape over hundreds of days. We therefore describe this transient evolution toward a 3D state with two time scales: a 30-day baroclinic adjustment followed by a 500+-day radiative adjustment period.

The slow adjustment time scale of our model is apparent from day 30 onward in Fig. 8 (as well as our subsequent figures showing transient evolution) as a slow and steady transition of contours toward an equilibrium 3D dynamical state. We find that tropospheric temperatures have nearly equilibrated after 100 days while the upper atmosphere continues to cool in the tropics and warm in the extratropics. Because the stratosphere has a much smaller optical depth than the troposphere, it can take a long time to reach a statistically steady state using explicit radiative transfer (such as our gray radiation) in a GCM. This behavior is made even more apparent by

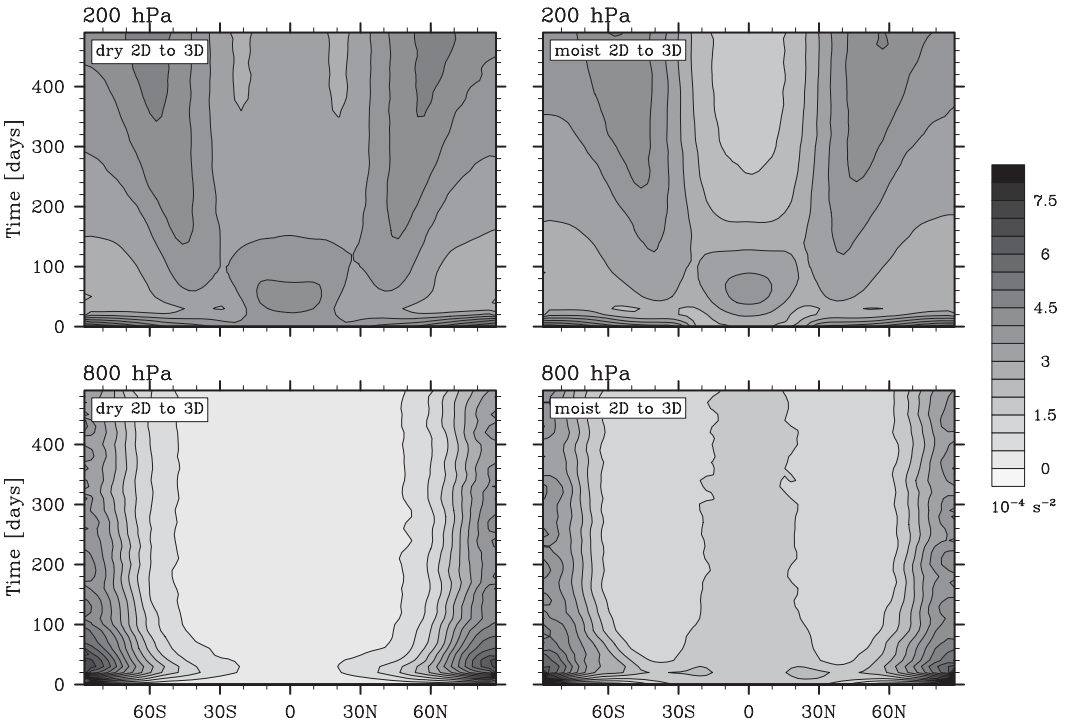

FIG. 9. Time evolution of $\overline{N}^2$ from the 2D to 3D dynamical state for an ensemble of calculations under (left) dry and (right) moist conditions at (top) 200 and (bottom) 800 hPa. Contours are drawn at an interval of 5×10^{-5} s^{-2}. Dashed contours mark negative values, and shading indicates $|\overline{N}^2|$.

the temporal evolution of $\overline{N}^2$, shown in Fig. 9, where the tropopause has reached a steady state after 500 days while the stratosphere continues to adjust.

The troposphere responds to eddies with a shorter baroclinic adjustment time scale. We magnify the first 100 days of evolution in Fig. 8, which shows two tropopause height pulses with midlatitude rising at 10 and 20 days. We associate these features with the life cycle of baroclinic waves as the atmosphere adjusts from a baroclinically unstable 2D state to a 3D state containing baroclinic eddies. The adjustment from 2D to 3D occurs relatively quickly and seems to require only two baroclinic life cycles for the troposphere to reach a 3D steady state. This time scale is consistent with existing theories for baroclinic adjustment in the atmosphere (e.g., Simmons and Hoskins 1978). It is also interesting to observe that $\overline{v'\theta'}$, shown in Fig. 10, has a maximum value at day 20 that seems to precede the rising of the tropopause at midlatitudes between days 20 and 200 in response to baroclinic waves. Additionally, $\overline{u'v'}$ shown in Fig. 11 has maxima near days 3 and 20 that coincide with the minimum heights in midlatitude tropopause height during baroclinic adjustment. We thus see that the troposphere responds to baroclinic eddies on a relatively rapid time scale, even though a steady-state atmosphere takes longer to develop.

We have argued in the section above that tropopause structure is affected by stratospheric cooling and warming that result in part from the Brewer–Dobson circulation. Although warming in the polar troposphere from sensible and latent heat fluxes causes tropopause heights to rise, the Brewer–Dobson circulation also causes stratospheric warming at polar latitudes. This exerts a competing force that lowers the polar tropopause so that the steady-state extratropical tropopause is determined by a competition of warming processes between tropospheric heat fluxes and stratospheric circulation.

The residual meridional circulation in the troposphere develops rather quickly and even persists during the initial 30-day baroclinic adjustment period. The temporal evolution of Ψ^* for dry and moist cases during the first 40 days of evolution in shown in Fig. 12 at heights of 200 and 800 hPa. This tropospheric circulation seems to develop immediately after eddies are introduced into the 2D state. By day 40 of evolution, this circulation in the troposphere is close to its steady-state strength.

The stratospheric Brewer–Dobson circulation, on the other hand, takes much longer to develop. The residual meridional circulation is shown in Fig. 12 out to 500 days of evolution, where it has evidently not yet reached a steady state. It is also interesting to note that the Brewer–Dobson circulation in the extratropical stratosphere takes

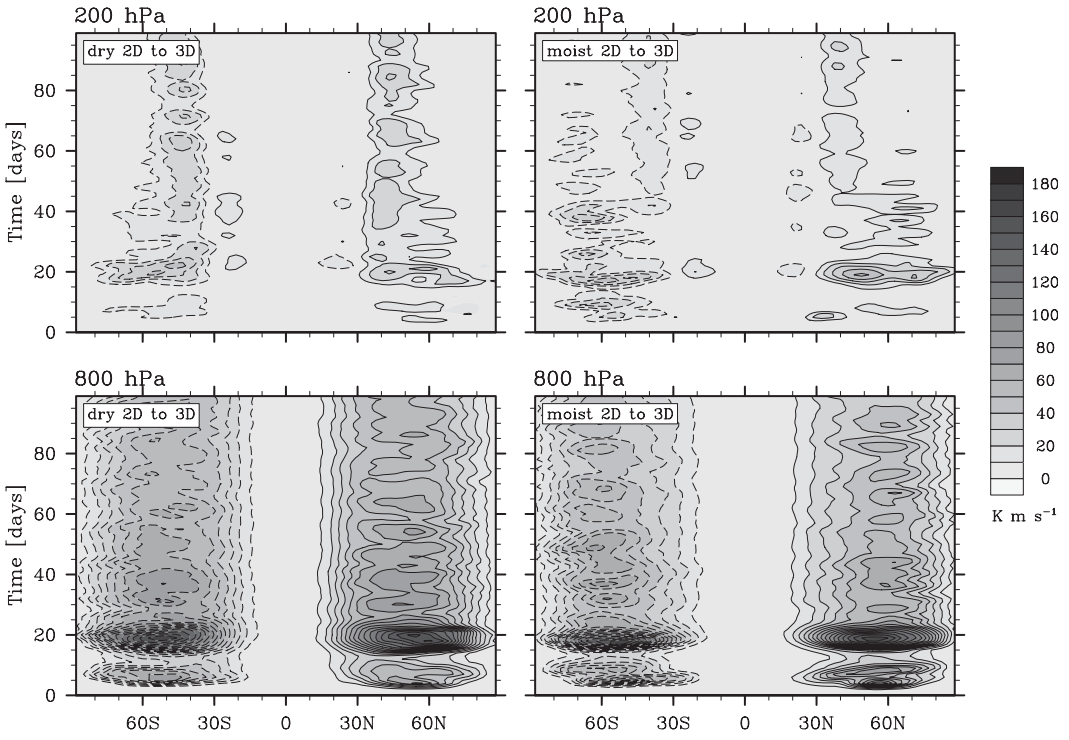

FIG. 10. Time evolution of $\overline{v'\theta'}$ from the 2D to 3D dynamical state for an ensemble of calculations under (left) dry and (right) moist conditions at (top) 200 and (bottom) 800 hPa. Contours are drawn at an interval of 10 K m s^{-1}.

a particularly long time to develop; our steady-state circulation shows poleward transport in Fig. 5, but this feature is still not present after 500 days of evolution in Fig. 12. As discussed above, radiative adjustment of the stratosphere occurs on a much longer time scale than the troposphere, so stratospheric processes should take longer to reach a steady state. [Part of this behavior relates to the stratospheric optical depth profile, described by Frierson et al. (2006), which can lead to a somewhat lengthy and unrealistic radiative time scale in the stratosphere.] As a result, we can explain the time evolution of the extratropical tropopause as a slow response to the developing temperature structure of the stratosphere.

We can now return to our hypothesis for tropopause structure, schematically illustrated in Fig. 6. The heating processes $\overline{\mathfrak{D}}$ and $\overline{Q}_{\text{norad}}$ have reached a near-steady state in the troposphere by about 100 days so that the resulting tropospheric poleward heat flux warms the poles and causes the tropopause to rise. Because this mechanism develops quickly, the extratropical tropopause rises significantly higher than its steady state when eddies are introduced. Only when the poleward warming of the stratosphere develops does the extratropical tropopause descend to eventually arrive at its final 3D configuration. Tropospheric evolution from 2D to 3D can therefore be understood as a competition between the rapid development of tropospheric latent and sensible heat fluxes and the slower development of stratospheric circulation.

6. Conclusions

The calculations presented in this paper indicate that the height of the tropopause is constrained not only by radiation and tropospheric eddy fluxes, but also by the stratospheric Brewer–Dobson circulation. Conventional wisdom assumes that the tropical tropopause is shaped by moist convection, but we find that a realistic tropopause profile, including a subtropical jump in height, can be maintained by eddies alone. Moist convection does contribute to overall higher tropical tropopause heights, but eddies seem to be the primary constraint on the shape of the tropical tropopause. Eddy-driven processes, including the stratospheric Brewer–Dobson circulation, modify atmospheric static stability so that the tropopause rises in the tropics and sharpens at the subtropics.

The extratropical tropopause is known to be shaped by baroclinic eddies (e.g., Held 1982; Lindzen 1993; Schneider 2004), but we find that moisture tends to flatten the extratropical tropopause in radiative regimes similar to that of the earth. In addition, eddies again play a central role in shaping the extratropical tropopause.

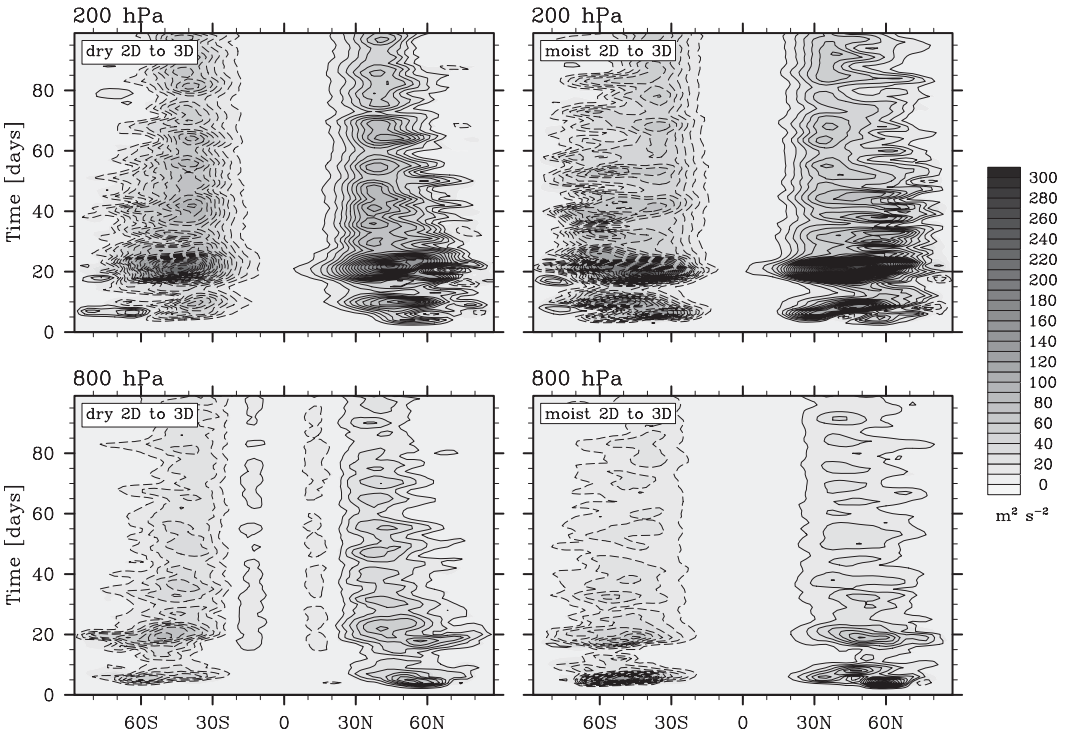

FIG. 11. As in Fig. 10, but for $\overline{u'v'}$. Contours are drawn at an interval of 10 m^2 s^{-2}.

Without stratospheric warming from eddies, the extratropical tropopause would be unrealistically higher than the observed tropopause. Under dry conditions the extratropical tropopause steepens due to eddies, while moist atmospheres have an additional poleward latent heat flux that causes flattening. Our interpretation is that the slope of the extratropical tropopause is determined by a competition between the tropospheric warming by eddy heat flux and the stratospheric warming by the Brewer–Dobson circulation and eddy-driven changes in upward infrared radiation. Thus, we find that baroclinic eddies significantly contribute to atmospheric structure in both the tropics and extratropics in large part by driving the Brewer–Dobson circulation to modify static stability.

Although our model configuration allows us to systematically isolate the effect of eddies, this GCM still contains idealized approximations that should be kept in mind. Because the surface is represented as an aquaplanet with a mixed-layer slab ocean, no large-scale planetary waves are induced (i.e., from interaction with topographic features). This aquaplanet approximation is necessary in this study in order to produce numerically stable RCE and 2D states, but it also leads to an underestimation of the Brewer–Dobson circulation strength because planetary waves can propagate into the stratosphere and break to strengthen this stratospheric circulation. This would not only produce a more realistic Brewer–Dobson circulation but also increase the effect of the Brewer–Dobson circulation on tropopause structure. Additionally, our use of perpetual equinox conditions prevents the Brewer–Dobson circulation from shifting off-axis to dominate the wintertime hemisphere, as would occur with a seasonal cycle for solar insolation. Likewise, the lack of water vapor feedback in our gray radiation scheme may cause an underestimation in the strength of tropical heating, while the lack of wavelength-dependent absorption for individual atmospheric constituents may lead to an oversimplification of stratospheric structure. It would certainly be worthwhile to repeat some of the calculations in this study using a more complicated model that includes some of these additional physical features; however, the basic effect of eddies on tropopause structure should remain consistent with more complex models.

The effect of the stratospheric Brewer–Dobson circulation is often ignored when formulating theories of the tropopause. However, our model hierarchy demonstrates that the Brewer–Dobson circulation plays the dominant role in shaping the tropical tropopause and also contributes significantly to tropopause structure in the extratropics. It appears that while our atmosphere is thermally forced, some of its most salient features are eddy driven, with a stratospheric circulation that may play a much more important role than previously thought.

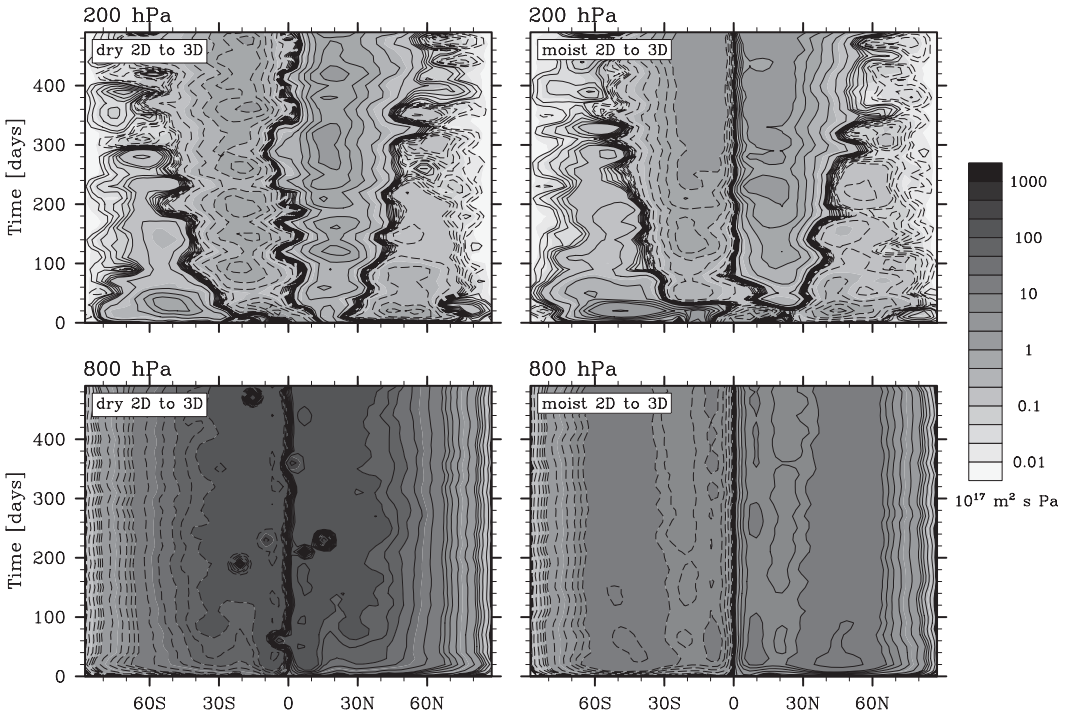

FIG. 12. Time evolution of Ψ^* for 500 days (10^{17} m^2 s Pa) from the 2D to 3D dynamical state for an ensemble of calculations under (left) dry and (right) moist conditions at (top) 200 and (bottom) 800 hPa. Contours are drawn irregularly according to $\pm\{1, 2, 4, 6, 8\} \times 10^n$, where $-2 \le n \le 4$, and dashed contours mark negative values. Shading follows the logarithmic scale on the side and indicates $|\Psi^*|$.

Acknowledgments. We thank Steven Feldstein for numerous discussions and suggestions that greatly strengthened this paper. DMWF is supported by NSF Grants ATM-0846641 and ATM-0936059.

REFERENCES

Ambaum, M., 1997: Isentropic formation of the tropopause. *J. Atmos. Sci.,* **54,** 555–568.

Anderson, J. L., and Coauthors, 2004: The new GFDL global atmosphere and land model AM2-LM2: Evaluation with prescribed SST simulations. *J. Climate,* **17,** 4641–4673.

Andrews, D. G., and M. E. McIntyre, 1976: Planetary waves in horizontal and vertical shear: The generalized Eliassen–Palm relation and the mean zonal acceleration. *J. Atmos. Sci.,* **33,** 2031–2048.

Austin, J., and F. Li, 2006: On the relationship between the strength of the Brewer–Dobson circulation and the age of stratospheric air. *Geophys. Res. Lett.,* **33,** L17807, doi:10.1029/2006GL026867.

Barry, L., G. C. Craig, and J. Thuburn, 2000: A GCM investigation into the nature of baroclinic adjustment. *J. Atmos. Sci.,* **57,** 1141–1155.

Betts, A. K., 1986: A new convective adjustment scheme. Part I: Observational and theoretical basis. *Quart. J. Roy. Meteor. Soc.,* **112,** 677–691.

Birner, T., 2010: Residual circulation and tropopause structure. *J. Atmos. Sci.,* **67,** 2582–2600.

——, A. Dörnbrack, and U. Schumann, 2002: How sharp is the tropopause at midlatitudes? *Geophys. Res. Lett.,* **29,** 1700, doi:10.1029/2002GL015142.

Bordi, I., A. Dell'Aquila, A. Speranza, and A. Sutera, 2002: Formula for a baroclinic adjustment theory of climate. *Tellus,* **54,** 260–272.

Brewer, A. W., 1949: Evidence for a world circulation provided by the measurements of helium and water vapour distribution in the stratosphere. *Quart. J. Roy. Meteor. Soc.,* **75,** 351–363.

Callaghan, P. F., and M. L. Salby, 2002: Three-dimensionality and forcing of the Brewer–Dobson circulation. *J. Atmos. Sci.,* **59,** 976–991.

Dell'Aquila, A., P. M. Ruti, and A. Sutera, 2007: Effects of the baroclinic adjustment on the tropopause in the NCEP–NCAR reanalysis. *Climate Dyn.,* **28,** 325–332.

Edmon, H. J., B. J. Hoskins, and M. E. McIntyre, 1980: Eliassen–Palm cross sections for the troposphere. *J. Atmos. Sci.,* **37,** 2600–2616.

Egger, J., 1995: Tropopause height in baroclinic channel flow. *J. Atmos. Sci.,* **52,** 2232–2241.

Eliassen, A., and E. Palm, 1961: On the transfer of energy in stationary mountain waves. *Geofys. Publ.,* **22,** 1–23.

Emanuel, K., 1994: *Atmospheric Convection*. Oxford University Press, 580 pp.

Frierson, D. M. W., 2007: The dynamics of idealized convection schemes and their effect on the zonally averaged tropical circulation. *J. Atmos. Sci.,* **64,** 1959–1976.

——, I. M. Held, and P. Zurita-Gotor, 2006: A gray-radiation aquaplanet moist GCM. Part I: Static stability and eddy scale. *J. Atmos. Sci.,* **63,** 2548–2566.

——, ——, and ——, 2007: A gray-radiation aquaplanet moist GCM. Part II: Energy transports in altered climates. *J. Atmos. Sci.,* **64,** 1680–1693.

Gabriel, A., G. Schmitz, and R. Geprägs, 1999: The tropopause in a 2D circulation model. *J. Atmos. Sci.,* **56,** 4059–4068.

Gordon, C. T., and W. F. Stern, 1982: A description of the GFDL global spectral model. *Mon. Wea. Rev.,* **110,** 625–644.

Gutowski, W. J., 1985: A simple model for the interaction between vertical eddy heat fluxes and static stability. *J. Atmos. Sci.,* **42,** 346–358.

——, L. E. Branscome, and D. A. Stewart, 1992: Life cycles of moist baroclinic eddies. *J. Atmos. Sci.,* **49,** 306–319.

Haqq-Misra, J., 2010: A dynamical hierarchy for the general circulation. Ph.D. thesis, The Pennsylvania State University, 200 pp.

Haynes, P., J. Scinocca, and M. Greenslade, 2001: Formation and maintenance of the extratropical tropopause by baroclinic eddies. *Geophys. Res. Lett.,* **28,** 4179–4182.

Held, I. M., 1982: On the height of the tropopause and the static stability of the troposphere. *J. Atmos. Sci.,* **39,** 412–417.

——, and M. J. Suarez, 1994: A proposal for the intercomparison of the dynamical cores of atmospheric general circulation models. *Bull. Amer. Meteor. Soc.,* **75,** 1825–1830.

Highwood, E. J., and B. J. Hoskins, 2006: The tropical tropopause. *Quart. J. Roy. Meteor. Soc.,* **124,** 1579–1604.

Hoerling, M. P., T. K. Schaack, and A. J. Lenzen, 1991: Global objective tropopause analysis. *Mon. Wea. Rev.,* **119,** 1816–1831.

Hoinka, K. P., 1998: Statistics of the global tropopause pressure. *Mon. Wea. Rev.,* **126,** 3303–3325.

Holton, J. R., P. H. Haynes, M. E. McIntyre, A. R. Douglass, R. B. Rood, and L. Pfister, 1995: Stratosphere–troposphere exchange. *Rev. Geophys.,* **33,** 403–439.

Kirk-Davidoff, D. B., and R. S. Lindzen, 2000: An energy balance model based on potential vorticity homogenization. *J. Climate,* **13,** 431–448.

Lindzen, R. S., 1993: Baroclinic neutrality and the tropopause. *J. Atmos. Sci.,* **50,** 1148–1151.

Manabe, S., and R. F. Strickler, 1964: Thermal equilibrium of the atmosphere with a convective adjustment. *J. Atmos. Sci.,* **21,** 361–385.

——, and R. T. Wetherald, 1967: Thermal equilibrium of the atmosphere with a given distribution of relative humidity. *J. Atmos. Sci.,* **24,** 241–259.

——, J. Smagorinsky, and R. F. Strickler, 1965: Simulated climatology of a general circulation model with a hydrologic cycle. *Mon. Wea. Rev.,* **93,** 769–798.

Pan, L. L., W. J. Randel, B. L. Gary, M. J. Mahoney, and E. J. Hintsa, 2004: Definitions and sharpness of the extratropical tropopause: A trace gas perspective. *J. Geophys. Res.,* **109,** D23103, doi:10.1029/2004JD004982.

Schneider, T., 2004: The tropopause and the thermal stratification in the extratropics of a dry atmosphere. *J. Atmos. Sci.,* **61,** 1317–1340.

——, and P. A. O'Gorman, 2008: Moist convection and the thermal stratification of the extratropical troposphere. *J. Atmos. Sci.,* **65,** 3571–3583.

Seidel, D. J., and W. J. Randel, 2006: Variability and trends in the global tropopause estimated from radiosonde data. *J. Geophys. Res.,* **111,** D21101, doi:10.1029/2006JD007363.

——, and ——, 2007: Recent widening of the tropical belt: Evidence from tropopause observations. *J. Geophys. Res.,* **112,** D20113, doi:10.1029/2007JD008861.

Simmons, A. J., and B. J. Hoskins, 1978: The life cycles of some nonlinear baroclinic waves. *J. Atmos. Sci.,* **35,** 414–432.

Son, S. W., S. Lee, and S. B. Feldstein, 2007: Intraseasonal variability of the zonal-mean extratropical tropopause height. *J. Atmos. Sci.,* **64,** 608–620.

Stohl, A., and Coauthors, 2003: Stratosphere–troposphere exchange: A review, and what we have learned from STACCATO. *J. Geophys. Res.,* **108,** 8516, doi:10.1029/2002JD002490.

Thuburn, J., and G. C. Craig, 1997: GCM tests of theories for the height of the tropopause. *J. Atmos. Sci.,* **54,** 869–882.

——, and ——, 2000: Stratospheric influence on tropopause height: The radiative constraint. *J. Atmos. Sci.,* **57,** 17–28.

Wirth, V., 2003: Static stability in the extratropical tropopause region. *J. Atmos. Sci.,* **60,** 1395–1409.

——, and T. Szabo, 2007: Sharpness of the extratropical tropopause in baroclinic life cycle experiments. *Geophys. Res. Lett.,* **34,** L02809, doi:10.1029/2006GL028369.

WMO, 1957: Definition of the tropopause. *WMO Bull.,* **6,** 136.

Xu, K. M., and K. A. Emanuel, 1989: Is the tropical atmosphere conditionally unstable? *Mon. Wea. Rev.,* **117,** 1471–1479.